Evidence for crisis-induced intermittency during geomagnetic superchron transitions

Breno Raphaldini,[1] David Ciro,[1] Everton S. Medeiros,[2] Lucas Massaroppe,[1] and Ricardo I. F. Trindade[1]
[1]*Institute of Astronomy, Geophysics and Atmospheric Sciences, University of São Paulo, Rua do Matão 1226, 05508-090 São Paulo, São Paulo, Brazil*
[2]*Institute of Physics, University of São Paulo, Rua do Matão 187, 05508-090 São Paulo, São Paulo, Brazil*

(Received 28 May 2019; revised manuscript received 12 November 2019; accepted 27 January 2020; published 12 February 2020)

The geomagnetic field's dipole undergoes polarity reversals in irregular time intervals. Particularly long periods without reversals (of the order of 10^7 yr), called superchrons, have occurred at least three times in the Phanerozoic (since 541 million years ago). We provide observational evidence for high non-Gaussianity in the vicinity of a transition to and from a geomagnetic superchron, consisting of a sharp increase in high-order moments (skewness and kurtosis) of the dipole's distribution. Such an increase in the moments is a universal feature of crisis-induced intermittency in low-dimensional dynamical systems undergoing global bifurcations. This implies a temporal variation of the underlying parameters of the physical system. Through a low-dimensional system that models the geomagnetic reversals, we show that the increase in the high-order moments during transitions to geomagnetic superchrons is caused by the progressive destruction of global periodic orbits exhibiting both polarities as the system approaches a merging bifurcation. We argue that the non-Gaussianity in this system is caused by the redistribution of the attractor around local cycles as global ones are destroyed.

DOI: 10.1103/PhysRevE.101.022206

I. INTRODUCTION

The geomagnetic field is generated by a dynamo process that takes place in the Earth's outer core. It is characterized by a strong dominant axial dipole, its polarity reversing in irregular time intervals that range from orders of $\sim 1 \times 10^4$ to 5×10^7 yr. Longer periods without reversals, of the order of 10^7 yr, are named geomagnetic superchrons and have occurred at least three times in the last 541 million years (Phanerozoic): the Cretaceous Normal Superchron, from about 120 to 83 million years ago, the Kiaman Reverse Superchron, from around 312 to 262 million years ago, and the Moyero Reverse Superchron, from 485 to 463 million years ago [1]. In the literature, there is no current consensus concerning the cause of such long quiet geomagnetic intervals. Some authors argue that these events may be generated by stationary chaotic and/or stochastic processes, implying that these events do not depend on eventual variations on physical parameters of the system [2]. Other authors argue that superchrons are caused by nonstationary processes, i.e., long-term variations of natural parameters that determine the dynamics of Earth's core, such as the evolution of the heat flux patterns and other physical characteristics of the core-mantle boundary [3,4]. Moreover, the question of whether there exists a paleomagnetic warning preceding a superchron is a long-standing question in the field of geomagnetism [5].

The data that can be used to tackle this open problem consist of paleomagnetic measurements of field directionality and intensity. Previous studies on this data have already unveiled important aspects of superchrons, for example, the existence of more stable geomagnetic field configuration during the superchrons [6] and low field intensities just before a superchron transition [7,8]. Additionally, some studies on geomagnetic dipole intensity indicate the existence of long-term trends, and possibly higher average values during superchrons [9]. Nevertheless, the causes of the observed absence of field reversals remain elusive.

In order to address these questions, we characterized the paleointensity measurements, given in virtual axial dipole moment (VADM) [10], by estimating the high-order moments of their statistical distribution. This particular approach is motivated by the ability of distribution moments in detecting nonstationary transitions, tipping points, in real-world [11] and theoretical [12,13] dynamical systems. Additionally, the high-order distribution moments have been used to investigate the departure from Gaussianity in ensembles of intrinsically chaotic solutions. This is particularly useful for characterizing the level of uncertainties in these systems [14].

In this work, we consider the third- and fourth-order distribution moments, namely, kurtosis and skewness, for time intervals of the paleointensity data of the geomagnetic field. We find that the transitions from and to superchrons are associated with a sharp increase of these statistical indicators near the beginning and end of the superchron, which strongly supports the hypothesis of nonstationary and bifurcation-related mechanisms for this scenario. Additionally, we show that both statistical moments, skewness and kurtosis, also have a sharp increase before a nonstationary transition from a reversing to a nonreversing state in a low-order dynamical model for dipole intensity. Such a relation between low-dimensional dynamical systems and the infinite-dimensional hydromagnetic problem is supported by estimates on the dimension of the attractor from paleointensity data, which indicates a low-dimensional intrinsic dynamics of the geomagnetic axial dipole [15].

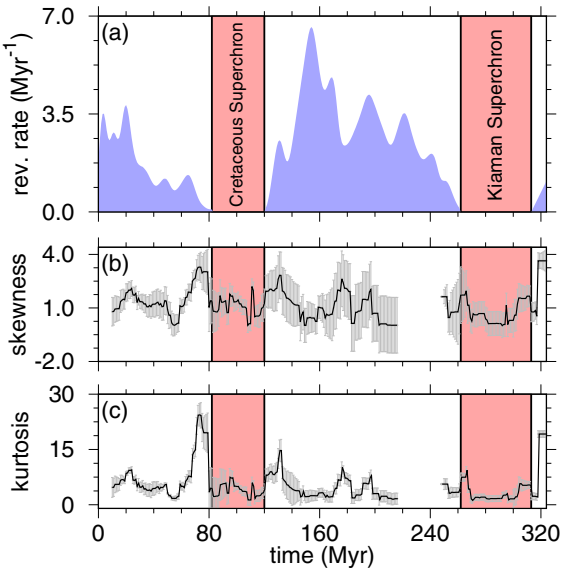

FIG. 1. (a) Geomagnetic reversal rates per million years according to the PINT database in the last 320 million years. The time intervals marked in red correspond to the superchrons. (b) The skewness obtained for a sliding window of size $\delta = 2$ million years. (c) The kurtosis obtained for the same sliding window of (b). Notice the beginning and the end of a superchron episode is accompanied by a peak of the skewness and kurtosis.

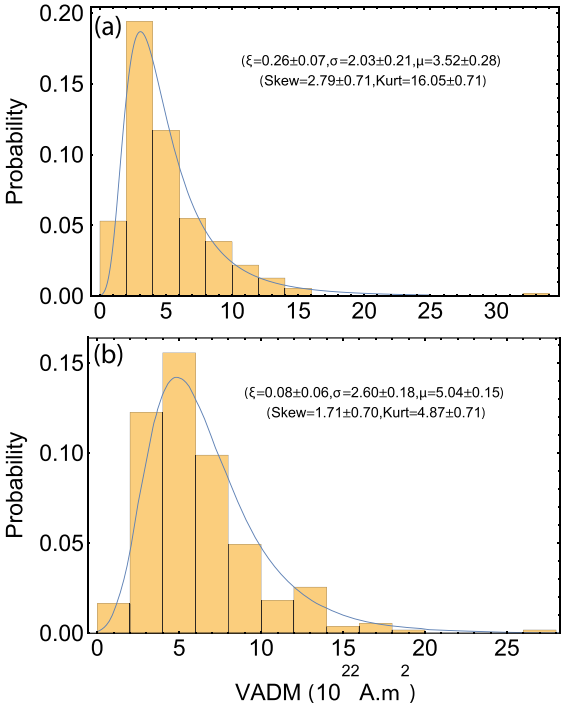

FIG. 2. Histograms of the paleointensities (VADM) in two different geodynamo regimes with a GEV probability density function adjusted: (a) Low reversal rates measured near the transition to a superchron with the respective GEV parameters. The higher values of kurtosis and skewness indicate that the system is approaching a transition. (b) Absence of reversals during the superchron. In this case, the reduction of the parameter ξ of the GEV distribution indicates a faster decaying tail. Notice the lower values of kurtosis and skewness. The adjusted statistical parameters are accompanied by 95% confidence intervals. The paleointensity measurements are given in A m^2.

Finally, we demonstrate that the variations of the high-order moments in the low-dimensional model are associated with the systematic destruction of global unstable periodic orbits preceding the global bifurcation where the field reversal ceases. Here, the sequential destruction of cycles leads to the redistribution of the flow along the chaotic attractor, under the control of previously less influential cycles, causing the observed changes in the distribution function momenta.

II. OBSERVATIONAL EVIDENCE FOR CRITICAL TRANSITIONS LEADING TO SUPERCHRONS

The PINT database is a compilation of paleomagnetic measurements by various authors corresponding to the last 3 billion years [16]. In order to characterize the geomagnetic field during transitions to superchrons, we analyzed the third (skewness) and fourth (kurtosis) moments of statistical distributions of the geomagnetic field intensity. These high-order distribution moments have been already associated with the proximity to nonstationary transitions [17]. Despite of eventual difficulties in precisely defining the exact location of transitions for oscillating trajectories [18,19], they proved to be useful in different contexts [11–13,20–22].

Now, in the paleomagnetic measurements, we assume that the parameters that determine the geodynamo evolution are approximately constant in a timescale of a few million years, a reasonable assumption given that the timescale for the convection of Earth's mantle is at least one order of magnitude greater [23]. Then, we calculate the moments at a given moment T, by averaging over all data in a time window $[T - \delta, T + \delta]$. Hence, in Figs. 1(b) and 1(c), we respectively show the skewness and the kurtosis for $\delta = 2$ million years. The conspicuous peaks in both skewness and kurtosis appearing before and after both superchrons shown in Fig. 1(a) are compelling evidence of the nonstationarity of these events. The applied statistical analysis is stable under the variation of δ. In order to estimate the confidence level of these results, we have employed a jackknife procedure that provides 95% confidence intervals.

The variations in the distribution moments observed in Fig. 1 indicate that during the transition from a normal reversing geodynamo state to a superchron, or vice versa, the statistical distribution is fat-tailed and skewed to the left. These measurements deviate significantly from the Gaussian distribution (kurtosis $= 3$ and skewness $= 0$), implying that such transitions are preceded by a higher frequency of extreme events in the geomagnetic field dipole intensity. Now, to further illustrate the fat-tailedness and the asymmetry of the intensity distribution near the transition, in Fig. 2 we show histograms of paleointensities in two regimes:

(i) Near the superchron transition, the frequency of extreme events in the field intensity increases (higher kurtosis) and its distribution becomes asymmetrical (higher skewness).

(ii) During the superchron (no reversals), the field intensity is known to be more stable; this fact is reflected in our analysis by a relatively low value of kurtosis and skewness.

Besides the statistical moments analysis, we have fitted a generalized extreme value (GEV) distribution to the data; we show that the shape parameter ξ of the GEV distribution drops to lower values in the superchron, which may be regarded as evidence for a fatter-tailed distribution near the transition to a superchron. However, the reason why it does not change its sign, as in Ref. [24], is explained at the end of the next section.

III. LOW-DIMENSIONAL DYNAMICAL SYSTEM ANALYSIS

Low-order dynamo models have been a valuable tool due to their simplicity for the understanding of natural dynamos and reversal processes [2,25–27]. In order to interpret the sharp increase in high-order moments during a regime transition in the geodynamo, we used a low-order model for geomagnetic field reversals consisting of a set of three nonlinearly coupled ordinary differential equations introduced in Ref. [28] and further analyzed in Ref. [29]. This model was derived by a low-order truncation combined with symmetry arguments. Additionally, a similar version of these equations with complex variables can be derived using different truncation arguments [30]. Although this kind of approximation of the infinite-dimensional magnetohydrodynamic equations may appear too drastic, this system keeps relevant qualitative features of the observed geodynamo [29]. This argument is additionally supported by estimates on the dimension of the attractor from paleointensity data indicating a low-dimensional nature of the geomagnetic axial dipole dynamics [15]. A more detailed discussion on the approximation of dissipative continuous systems, like the magnetohydrodynamic equations governing the geodynamo, by appropriate three-dimensional dynamical systems can be found in Ref. [31].

The three-dimensional system of differential equations involves the magnetic dipole component D, the magnetic quadrupole Q, which is believed to be crucial in the reversal process [32,33], and a velocity field mode V that is antisymmetric to the equatorial plane [34]. These equations take the form

$$\dot{Q} = \mu Q - VD, \quad \dot{D} = -\nu D + VQ, \quad \dot{V} = \Gamma - V + QD, \tag{1}$$

where the nondimensional parameters $\{\mu, \nu, \Gamma\}$ represent the instability growth rate acting on the quadrupole Q, the energy dissipation parameter acting on the dipole D, and forcing on the symmetry breaking velocity field component V, respectively. Each component is coupled to the other two via quadratic nonlinear terms (see Refs. [28,29] for more details). Despite the simplicity of this model, it presents very rich dynamics and remarkable resemblance with the observed behavior of geomagnetic reversals, with irregular polarity switches, overshooting of the intensities during a reversal, and a polarity statistics that is approximately Poissonian and a very rich array of dynamical regimes. In Ref. [28] the authors show that this model is able to correctly capture the morphology and the qualitative aspects of the energy transfers of full dynamo simulations at low magnetic Prandtl number. Recently, this and a few other simple models were used in Ref. [35] to perform data assimilation with geomagnetic field measurements to provide an estimate of the expected time for the next geomagnetic reversal, and this model was found to be the one that best represents the reversal process. The only drawback of this model according to the authors of Ref. [35] is related to its lack of fast fluctuations; this could be improved by including more velocity field modes in the equations (for instance coupling these equations to a turbulent shell model as in Ref. [25]). The equations describing the model have been integrated by a Runge-Kutta-Fehlberg algorithm with an adaptive step size. Although the statistical properties of interest here do not depend upon a particular initial condition, for all our simulations, the trajectories started at $(-2, 2, -2)$. After a transient time has been discarded, we consider 10^6 trajectory points to calculate the statistical moments.

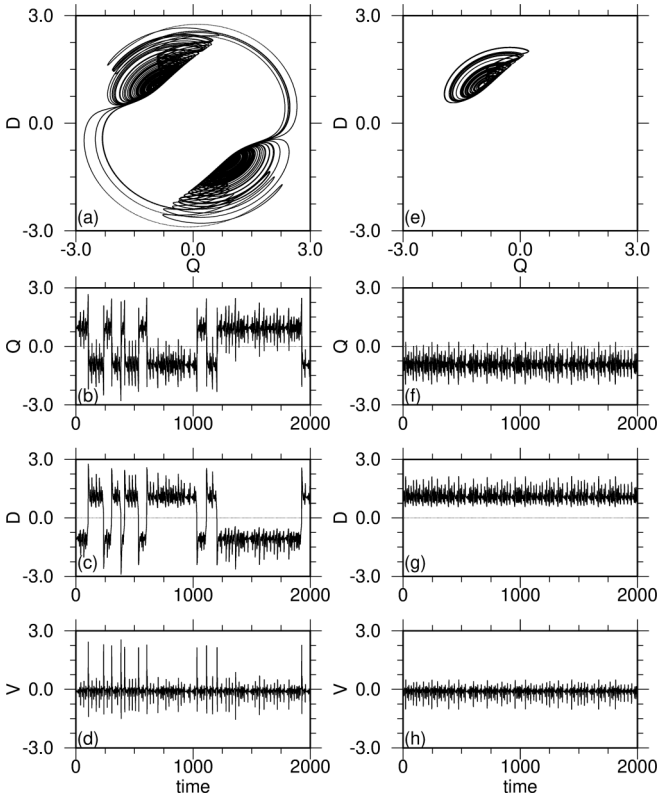

FIG. 3. (a)–(d) The control parameters are fixed at $\mu = 0.1189$, $\nu = 0.1$, and $\Gamma = 0.9$. The model [Eq. (1)] presents field reversals as shown in (a) two-dimensional phase space projection ($Q \times D$), (b) time evolution of the quadrupole component Q, (c) time evolution of the dipole variable D, and (d) time evolution of velocity field component. (e)–(h) The control parameters are fixed at $\mu = 0.12$, $\nu = 0.1$, and $\Gamma = 0.9$. The model is reversal free.

We present solutions of this model for two different regimes. First, we obtain the field reversal dynamics by setting the control parameters at $\mu = 0.1189$, $\nu = 0.1$, and $\Gamma = 0.9$ [see Figs. 3(a)–3(d)]. In Fig. 3(a), we show a two-dimensional ($Q \times D$) projection of the system phase space illustrating the behavior of the dipole variable D as a function of the quadrupole component Q. From Figs. 3(b) and 3(c), we observe that the dipole variable D displays aperiodic changes of polarity in antiphase with the quadrupole component Q. Both modes (Q, D) of the magnetic field are coupled via the velocity field component V that displays a very intermittent

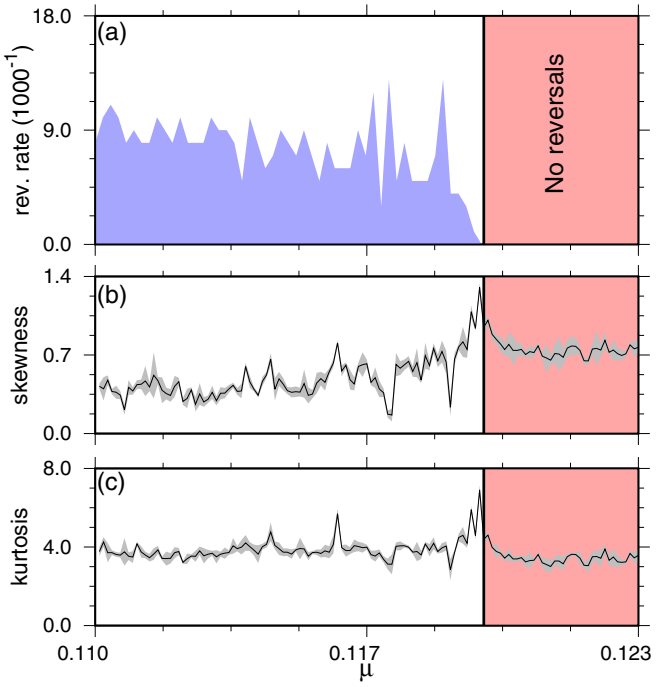

FIG. 4. (a) The reversal rates obtained for every 1000 (arb. units) of the time evolution. (b) The corresponding skewness and (c) the kurtosis. Analogously to the observational results of paleomagnetic measurements, an increase in kurtosis and skewness occurs before the transition. The gray shading in (b) and (c) represents the confidence interval of the corresponding statistical moments. The parameters are fixed at $\nu = 0.1$, $\Gamma = 0.9$, and $\mu \in [0.110, 0.123]$.

behavior shown in Fig. 3(d). Next, we obtain a reversal-free evolution of the model by only resetting the parameter μ at 0.12 [Figs. 3(e)–3(h)].

Therefore, one clear advantage of this reduced model of geomagnetic reversals over others is its ability to reproduce the transitions from superchrons to a normal reversing dynamo state by varying one parameter of the system as first reported in Ref. [29]. This is a nonstationary transition well characterized in bifurcation theory as a crisis-induced intermittency [36]. Additionally, early warnings for this kind of global bifurcation involving chaotic attractors have been recently addressed in the literature [37].

Here, we aim to establish a connection between the statistical results obtained for the paleomagnetic measurements of the geomagnetic field with the nonstationary crisis-induced intermittency occurring in the model described by Eq. (1). For that, we investigated the behavior of the model during the crisis-induced intermittency in an inverse merging bifurcation, which corresponds to the transition to a superchron in the paleomagnetic measurements. Hence, in Fig. 4(a), the aforementioned model was integrated numerically for 200 different values of the dissipation rate μ. For every value of μ, we integrated the system for $t = 1000$ (arb. units) and computed the model reversal rate during this time interval. The reversal rate corresponds to the number of inversions performed by the dipole intensity of the system between two symmetric portions of a chaotic attractor. Next, for every value of μ, we calculated the kurtosis and skewness of the distribution generated by the model dipole intensity during a time interval of $t = 1000$ (arb. units). Notice that, in Figs. 4(b) and 4(c), there is a sharp increase in both moments when μ reaches a critical value μ_c, at which the transition from a reversing state to a nonreversing state, or superchron, occurs.

The behavior of the statistical moments across the critical value observed in Fig. 4 resemble the previously described changes in the third and fourth moments on the paleointensity measurements. These observations suggest the existence of a common mechanism between the reduced model and the geodynamo. Another common feature between the geodynamo and the reduced model is that there can be increases in the third and fourth moments of the dipole intensity away from the critical time or parameters, respectively, but such peaks appear for shorter periods or small parametric windows and will be linked to another type of local bifurcation in the next section.

We end this section by discussing the application of extreme value theory indicators to this particular system. As suggested in Ref. [24], the shape parameter of the GEV distribution serves as an indicator that the system is approaching a crisis. The applicability of this concept was demonstrated in Ref. [21] to evaluate turbulent transitions in a Couette flow. It was subsequently applied in the context of experimental liquid sodium dynamos [38], where extreme value theory was used as an indicator for the dynamo threshold as a function of the magnetic Reynolds number. The idea behind the use of a GEV shape parameter as an indicator of a crisis comes from the fact that for dynamical systems satisfying axiom A [39], fluctuations should be bounded in such a way that extreme events are better described by a Weibull-type distribution (a GEV distribution with $\xi < 0$). As discussed in section 11.5 of Ref. [40], the situation can be more delicate when applying this theory to dynamical systems with rare transitions between two separate regions of the attractor. In this situation one may expect the dynamics on a short timescale, when the orbit is situated in one of the scrolls, to be well approximated by an axiom-A-type of system, with periodic orbits being dense in this bounded region of the attractor. However, this behavior is violated by the rare transitions that occur between the two regions of the attractor, such that the laws for the extremes violate a Weibull type of distribution.

We performed long integrations of the model (10^5 model time units) and fitted GEV distributions to the block maxima time series. In our analysis, we find the GEV shape parameter for the D variable to be positive throughout the crisis ($\xi_\mu > 0$); however, we observe that the bistability of the system can only be appreciated in the D-Q plane. When we evaluated the variation of the GEV shape parameter for the velocity variable V, we were able to observe ξ changing sign exactly at the critical value μ_c. This makes the transition from bounded oscillations ($\xi < 0$), characterizing a Weibull distribution, to a regime with unbounded oscillations associated with a Fréchet type of distribution (see Fig. 5). This implies that although the system probably violates axiom A [41,42] for both $\mu < \mu_c$ and $\mu > \mu_c$ (for the range of μs studied), the invariant measure of the system when marginalized for the variable V does not see the unboundedness of the tail before the crisis but is able to capture these rare excursions after the crisis. In fact, on closer inspection, we observe that the segments of

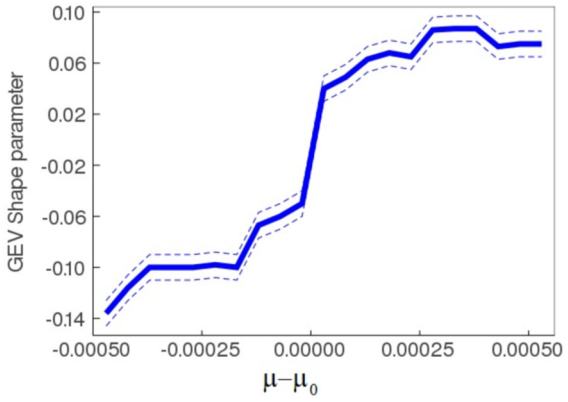

FIG. 5. The shape parameter ξ as a function of the distance of the control parameter μ to its critical value μ_c. The shape parameter ξ changes sign during the transition as predicted by the theory. The dashed curves represent the confidence interval of the corresponding GEV values. The other parameters of the model are fixed at $\nu = 0.1$ and $\Gamma = 0.9$.

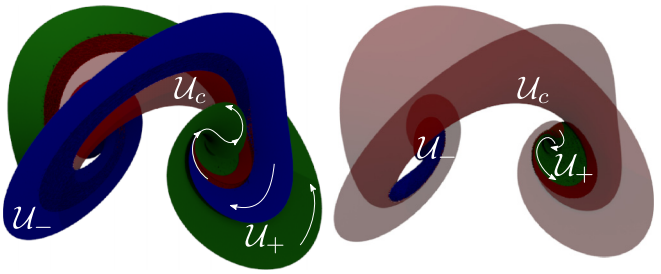

FIG. 6. Unstable manifolds of D_- (blue), D_+ (green), and C (red) in a reversing case $\mu = 0.1189 < \mu_c$ (left) and a nonreversing case $\mu = 0.12 > \mu_c$ (right). In the reversing case, the unstable manifolds of D_+ and D_- become interwinded, resulting in orbits that transit both regions of phase space, in contrast to the nonreversing case where the manifolds are confined on each side, resulting in orbits that do not reverse polarity. In both situations, the unstable manifold of C winds about both sides of the attractor diverting orbits coming from far in phase space. The other parameters are fixed at $\nu = 0.1$ and $\Gamma = 0.9$.

orbits that perform a reversal in the model correspond to large fluctuations in V. This also suggests that there are two types of extreme events in this system, one of them being transversal to the D-Q plane.

IV. STATISTICAL MOMENTS AND THE DESTRUCTION OF GLOBAL UNSTABLE PERIODIC ORBITS

To better elucidate the mechanisms behind the increase in the third and fourth statistical moments we need to investigate the structure of the phase space before and after a transition. For the values of the parameters considered here, the system has three fixed points: one in the V axis labeled C, and two symmetric ones with positive and negative values of D, which we label D_- and D_+. All the fixed points are saddles, with a one-dimensional stable manifold and a two-dimensional unstable manifold. In this model, a transition of the orbit from the vicinity of D_+ to the vicinity of D_- constitutes a reversal of the system and the saddle C only diverts orbits that come from far locations towards D_+ or D_-. In the nonreversing "superchron" state the system has two separated basins of attraction, comprising the positive and negative D states.

In general, chaotic orbits are driven far from the saddles by the unstable manifolds $W^u(D_+, D_-)$ and attracted back by their one-dimensional stable manifold. This simple process generates an intricate set of closed orbits, or unstable periodic orbits (UPOs), which are periodic solutions of the differential equations and have associated two-dimensional stable and unstable manifolds, in a similar fashion to the mentioned saddle points (Fig. 6). Chaotic orbits bounce back and forth between UPOs, getting attracted through their stable manifold and then repealed through the unstable one, spending different amounts of time near each UPO depending on its relative distance to the corresponding stable manifold. This process causes the UPOs to have an important influence on the phase-space distribution function since orbits tend to spend long times in their vicinity.

A first description of the phase-space structure can be made in terms of the manifolds of the saddles D_+, D_-, and C, which strongly influence the shape and extension of the UPOs. In the reversing state ($\mu < \mu_c$), both unstable manifolds $W^u(D_+)$ and $W^u(D_-)$ occupy a large region of the phase space and strongly interact by wrapping about each other in a complex helical spiral, as depicted in Fig. 6 (left), while in the nonreversing situation ($\mu > \mu_c$) (Fig. 6, right), the unstable manifolds $W^u(D_+)$ and $W^u(D_-)$ do not interact and are compactly wrapped about their corresponding saddles, separating the chaotic attractor in two pieces with different basins of attraction.

For a more detailed account of the phase-space distribution function, and, in particular, the dipoles' distribution, we turn to the study of UPOs of the dynamical system, which can be created and annihilated as the control parameters are changed. Transitional chaotic orbits are influenced by "global" UPOs, which access the vicinity of both antipodal fixed points (Fig. 7, left), and only exist below the critical value μ_c. For dissipation rates μ *far* below μ_c, the local and global UPOs are concentrated around $D+$ and D_-, leading to smaller values of the kurtosis and skewness. This changes as one approaches the critical value μ_c from below; global UPOs are sequentially destroyed, and new local and global UPOs wider in the dipole direction, with shorter life span in μ, are created in their place.

Since chaotic orbits tend to spend long times near the UPOs, each influential cycle causes an increase in the phase-space distribution function around it. When changing parameters, some UPOs can be destroyed by touching some stable manifold of another invariant structure, spreading this higher density to other regions of phase space. Such spreading leads to an increase in the distribution moments with respect to the previous situation with the underlying UPO.

This mechanism is quite general and explains the appearance of local peaks in the distribution moments away from the critical values in Figs. 2 and 4. Provided that all global UPOs must be destroyed before the critical value μ_c, this redistribution process occurs very frequently near the global bifurcation, leading to the increase in the global high-order distribution moments for a longer time or a larger parameter window. Additionally, short-lived global cycles created during

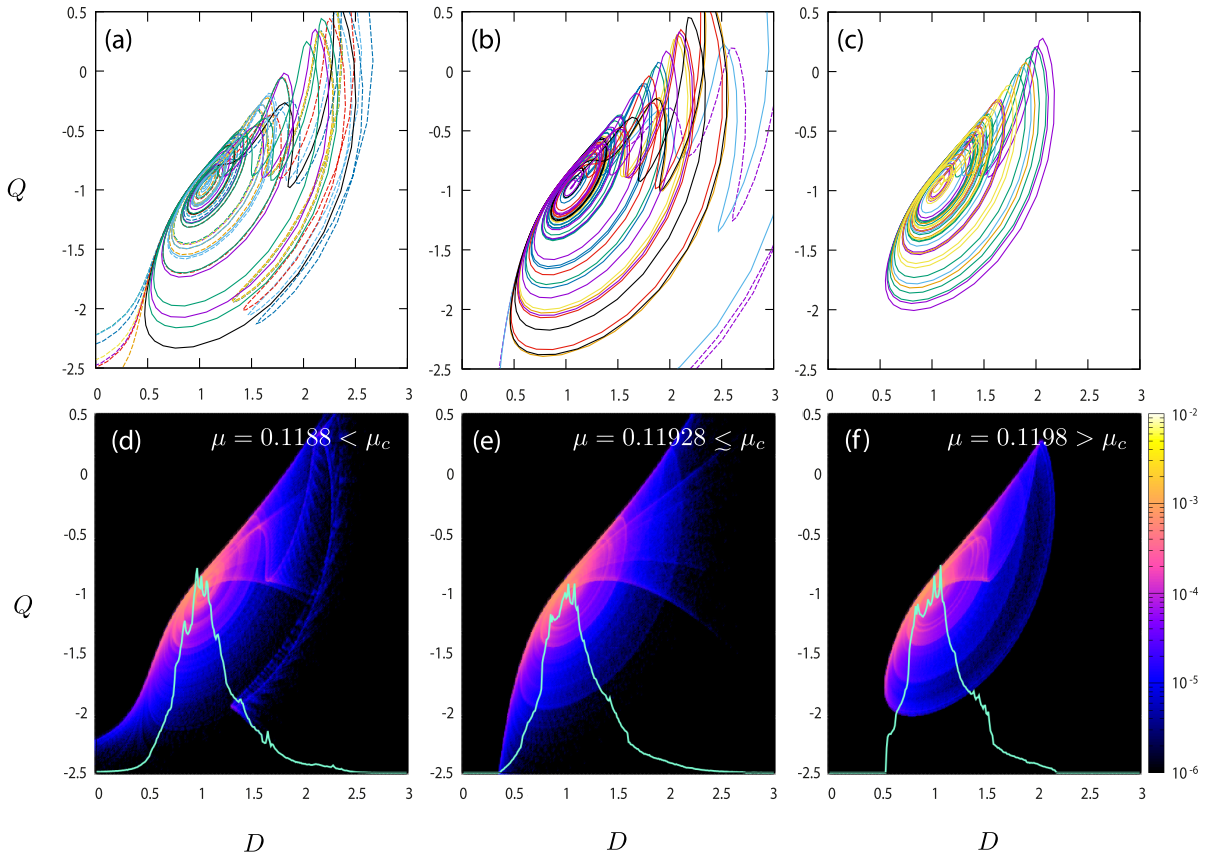

FIG. 7. A few dominant UPOs in the D-Q plane for (a) $\mu < \mu_c$, (b) $\mu \lesssim \mu_c$, and (c) $\mu > \mu_c$. (d)–(f) The associated two-dimensional (2D) histograms with their respective one-dimensional (1D) projection in the dipoles' space. Local UPOs [continuous lines in (a) and (b)] are mostly concentrated near $D_\pm$, while global UPOs [dashed lines in (a) and (b)] are responsible for transitions. Near the critical value μ_c in a reversing state new wider local and global UPOs generate extreme events, giving a fatter-tailed distribution when compared to μ far below or above μ_c. The other parameters are fixed at $\nu = 0.1$ and $\Gamma = 0.9$.

the transition are wider than their predecessors, contributing further to the spreading of the distribution function during the transition. Similar situations in which external UPOs that are usually invisible to the dynamics and become accessible through external forcing are described in other geophysical systems as in atmospheric dynamics (see Ref. [43]; see also Ref. [44] for further discussion on the role of the UPOs in the statistics of the atmospheric equations).

Wide UPOs also increase the occurrence of extreme events in the magnetic dipole D, leading to a broader and more skewed distribution function (Fig. 7, center). Local wide UPOs persist across μ_c, but global ones cannot exist above it. Thus, the wider distribution function is maintained by wide local UPOs until they get destroyed as we further increase μ. This is consistent with the subsequent decrease in the distribution moments of D, for $\mu > \mu_c$ as observed in Fig. 4. Correspondingly, the local UPOs are compact and uniformly distributed on the attractor (Fig. 4, right), in agreement with the small values of the kurtosis and skewness, which are maintained from here on.

V. CONCLUDING REMARKS

We have presented evidence for the occurrence of critical transitions just before and just after geomagnetic superchrons based on the sharp increase of the kurtosis and skewness of paleointensity geomagnetic data. This behavior is shown to be analogous to the one observed in a low-order model for geomagnetic reversals in which crisis-induced intermittency causes a shift of the system from a reversing state to a nonreversing one and presents the measured changes in the distribution moments of paleomagnetic data. This strongly suggests that the underlying mechanism that generates the transition to or from the superchron geomagnetic transitions is driven by changes in the physical parameters of the system instead of particularly long standings in a given polarity of a chaotic orbit. Physical parameters that evolve throughout the geological time such as temperature, thermal or electrical conductivity, or topography at the core-mantle boundary could constitute these parameters [45–47]. We argue that the mechanism proposed here to explain the sharp variation in the statistical moments is not strongly dependent on the particular low-dimensional model under consideration. Since type-one crisis-induced intermittency is defined by the merging of two (or more) separated attractors into one, it involves the interaction between invariant manifolds of different periodic orbits and fixed points. The sequential destruction of global UPOs near the transition leads to the redistribution of the higher distribution values around them, increasing the global kurtosis and also generating wider short-lived periodic

orbits which further increase this distribution moment and are asymmetric with respect to the antipodal points leading to a higher skewness. These moments also increase the evidence of the occurrence of more extreme events in the magnetic dipole intensity just before and after a transition to a superchron state. Besides more paleointensity and paleomagnetic data near the superchron transition, another interesting line of research that would help us understand reversals in natural dynamos is that of the experimental turbulent dynamos as in Ref. [48].

ACKNOWLEDGMENTS

This work was supported by FAPESP (Grants No. 2015/50686-1, No. 2017/23417-5, No. 2013/26598-0, and No. 2018/03211-6).

APPENDIX: SEARCHING AND TRACKING UPOS

Consider a dynamical system in the autonomous form

$$\frac{dx}{dt} = f(x), \tag{A1}$$

where $x \in \mathbb{R}^n$ and $f : \mathbb{R}^n \to \mathbb{R}^n$. The solution of the equations defining the dynamical system is the flow $\varphi : \mathbb{R}^n \times \mathbb{R} \to \mathbb{R}^n$, of the vector field f. This flow is such that $\varphi(x, t)$ is the position of the solution starting at x and evolving during a time t. The functional

$$S(x, t) = |\varphi(x, t) - x|^2 \tag{A2}$$

measures the distance between an initial condition x and the flow departing from it after a time t. Clearly, if x^* belongs to a periodic orbit of the dynamical system (A1), it satisfies $S(x^*, T) = 0$, where $T > 0$ is the time of first return or period of the orbit.

Provided that we have the means to produce $\varphi(x, t)$, the numerical determination of UPOs consists in the identification of pairs (x_i, T_i) for which the functional (A2) vanishes. Consider the collective variable $u \in \mathbb{R}^{n+1}$, such that $u_i = x_i$ for $i \in \{1, 2, \ldots, n\}$ and $u_{n+1} = t$. We want to minimize the functional

$$S(u) = \sum_{i=0}^{n} [\varphi_i(u) - u_i]^2. \tag{A3}$$

Following the Levenberg-Marquardt procedure we start from u^0 which is close to the desired solution u^*, then consider a small variation δu, such that $u_0 + \delta u = u^*$ causes $S(u^0 + \delta u)$ to become stationary respect to δu. This leads to an approximated equation for δu,

$$[A^T A - \lambda \mathrm{Diag}(A^T A)]\delta u = A^T [x - \varphi(u)], \tag{A4}$$

where $A_{i,j} = \partial\varphi_i/\partial u_j|_{u^0} - \delta_{i,j}$, and $i = 1, 2, \ldots, n$, $j = 1, 2, \ldots, n+1$. Diagonal damping is included to prevent overshooting and to scale appropriately the steps on each direction. Since (A4) is not exact, the procedure must be iterated until the functional goes below some tolerance value. Additionally, the scalar λ is an adaptive parameter that allows to control the velocity of convergence if the method approaches stagnation.

An important issue is the numerical determination of $\partial\varphi_i/\partial u_j|_{u_0}$, which are the elements of the monodromy matrix when the solution is periodic. This matrix can be obtained by integrating

$$\frac{dA}{dt} = J(x(t))A(x(t)), \tag{A5}$$

where $A(x(0))$ is the identity, $x(t)$ is a numerical solution of the system starting at $x(0) = x_0$, and J is the regular Jacobian of the flow. Finally, for the time derivative of the flow we have simply

$$\frac{\partial}{\partial t}\varphi(x, t) = f(\varphi(x, t), t). \tag{A6}$$

Provided that the reference orbit is sufficiently close to the UPO, Eq. (A5) should give a reasonable approximation of the monodromy matrix. An additional complication emerges near the UPO destruction, where the system (A5) becomes unstable and a special method of finite differences becomes more reliable and easier to implement.

1. Determining initial conditions

Provided that chaotic orbits are subsequently attracted to and repelled from different UPOs, the chaotic dynamics contain ordered sequences of the underlying periodic orbits. This mimicking allows us to use chaotic orbits to estimate the locations of UPOs and their periods. In principle, we can take N subsequent points that discretize a finite segment of the chaotic orbit and perform N^2 comparisons to see which points are separated in time and very close in distance. However, this can be extremely expensive and the following preselection process was implemented:

(1) Integrate the dynamical system from an arbitrary $x^\dagger$ for a very long time. Define $\varphi(t) = \varphi(x^\dagger, t)$.

(2) Determine the instants $\{t_i\}$ for which some appropriate component of the flow $\varphi_k(t_i)$ reaches a maximum value.

(3) Measure the distances $d_{i,j} = |\varphi(t_i) - \varphi(t_j)|$.

(4) If $d_{i,j} < \epsilon$ for some small ϵ and $j > i$, define the initial guess $u_0 = \{\bar{\varphi}_{i,j}, \Delta t_{i,j}\}$, with $\bar{\varphi}_{i,j} = [\varphi(t_i) + \varphi(t_j)]/2$ and $\Delta t_{i,j} = t_j - t_i$. Take the new i equal to $j + 1$ to prevent initial guesses that lead to the same orbit.

This method uses the simple fact that periodic orbits must contain subsequent maxima and minima in all its dynamical variables. Then we can take the maximum of any dynamical variable as the starting and ending point of the periodic orbit. If a chaotic orbit is mimicking this orbit it will develop two maxima in the same variable at approximately the same location, and the time between them will be a good initial guess of the period of the orbit. Additionally, by defining the initial guess using a reference chaotic orbit we ensure that the UPOs being tracked are the ones that really affect our dynamics the most so that they contribute the most to the statistical moments of the distribution function.

2. Tracking across parameters

Provided that we have determined an UPO for a given value of μ, we can take its period and *any* point in the orbit as an initial guess for determining the UPO in $\mu + \delta_m u$. However, UPOs can undergo important geometrical changes under small variations in the control parameters and even be destroyed, so special care must be devoted to tracking

these orbits in a sufficiently smooth fashion. To do this we take a relevant parameter of the orbit, e.g., its period $T(\mu)$, which must be a smooth function of the control parameter, and attempt to perform small fixed steps in such a parameter instead of μ, i.e., $T(\mu+\delta\mu) < T(\mu)+\delta T$, for some small fixed δT. Then for small $\delta\mu$ we have

$$\delta\mu \approx \delta T \left(\frac{dT}{d\mu}\right)^{-1}, \tag{A7}$$

i.e., we can estimate μ_{n+1} from two close previous values

$$\mu_{n+1} \approx \mu_n + \frac{\mu_n - \mu_{n-1}}{T_n - T_{n-1}}\delta T, \tag{A8}$$

where $T_n = T(\mu_n)$. For an appropriate choice of the period step δT there is a better chance of converging to the appropriate UPO, in contrast to just taking fixed steps in μ.

[1] J. A. Jacobs, Astron. Geophys. **42**, 6.30 (2001).
[2] D. A. Ryan and G. R. Sarson, Geophys. Res. Lett. **34**, L02307 (2007).
[3] P. Driscoll and P. Olson, Geophys. Res. Lett. **38**, L09304 (2011).
[4] F. Pétrélis, J. Besse, and J.-P. Valet, Geophys. Res. Lett. **38**, L19303 (2011).
[5] G. Hulot and Y. Gallet, Earth Planet. Sci. Lett. **210**, 191 (2003).
[6] T. Veikkolainen and L. J. Pesonen, Geophys. J. Int. **199**, 1515 (2014).
[7] R. Zhu, K. A. Hoffman, Y. Pan, R. Shi, and D. Li, Phys. Earth Planet. Inter. **136**, 187 (2003).
[8] R. Zhu, Y. Pan, J. Shaw, D. Li, and Q. Li, Phys. Earth Planet. Inter. **128**, 207 (2001).
[9] P. E. Driscoll and D. A. Evans, Earth Planet. Sci. Lett. **437**, 9 (2016).
[10] J.-P. Valet, L. Meynadier, and Y. Guyodo, Nature (London) **435**, 802 (2005).
[11] A. S. Gsell, U. Scharfenberger, D. Özkundakci, A. Walters, L.-A. Hansson, A. B. G. Janssen, P. Nõges, P. C. Reid, D. E. Schindler, E. Van Donk, V. Dakos, and R. Adrian, Proc. Natl. Acad. Sci. USA **113**, E8089 (2016).
[12] V. Guttal and C. Jayaprakash, Ecol. Lett. **11**, 450 (2008).
[13] S. Kéfi, V. Guttal, W. A. Brock, S. R. Carpenter, A. M. Ellison, V. N. Livina, D. A. Seekell, M. Scheffer, E. H. van Nes, and V. Dakos, PLoS ONE **9**, e92097 (2014).
[14] R. V. Abramov and A. J. Majda, SIAM J. Sci. Comput. **26**, 411 (2004).
[15] D. A. Ryan and G. R. Sarson, Europhys. Lett. **83**, 49001 (2008).
[16] A. J. Biggin and G. A. Paterson, Front. Earth Sci. **2**, 24 (2014).
[17] V. Dakos, S. R. Carpenter, W. A. Brock, A. M. Ellison, V. Guttal, A. R. Ives, S. Kéfi, V. Livina, D. A. Seekell, E. H. van Nes, and M. Scheffer, PLoS ONE **7**, e41010 (2012).
[18] E. S. Medeiros, I. L. Caldas, M. S. Baptista, and U. Feudel, Sci. Rep. **7**, 42351 (2017).
[19] S. Bathiany, M. Scheffer, E. H. van Nes, M. S. Williamson, and T. M. Lenton, Sci. Rep. **8**, 5040 (2018).
[20] S. M. S. Alam and M. I. H. Bhuiyan, IEEE J. Biomed. Health Inf. **17**, 312 (2013).
[21] D. Faranda, V. Lucarini, P. Manneville, and J. Wouters, Chaos Solitons Fractals **64**, 26 (2014).
[22] S. Orozco-Fuentes, G. Griffiths, M. Holmes, R. Ettelaie, J. Smith, A. Baggaley, and N. Parker, Ecol. Modell. **393**, 12 (2019).
[23] M. A. Richards and D. C. Engebretson, Nature (London) **355**, 437 (1992).
[24] D. Faranda, V. Lucarini, G. Turchetti, and S. Vaienti, Int. J. Bifurcation Chaos **22**, 1250276 (2012).
[25] R. Benzi and J.-F. Pinton, Phys. Rev. Lett. **105**, 024501 (2010).
[26] F. Pétrélis, S. Fauve, E. Dormy, and J.-P. Valet, Phys. Rev. Lett. **102**, 144503 (2009).
[27] D. Chillingworth and P. Holmes, J. Int. Assoc. Math. Geol. **12**, 41 (1980).
[28] C. Gissinger, E. Dormy, and S. Fauve, Europhys. Lett. **90**, 49001 (2010).
[29] C. Gissinger, Eur. Phys. J. B **85**, 137 (2012).
[30] B. Raphaldini and C. F. M. Raupp, Astrophys. J. **799**, 78 (2015).
[31] J. C. Robinson, Nonlinearity **11**, 529 (1998).
[32] D. Gubbins and K. Zhang, Phys. Earth Planet. Inter. **75**, 225 (1993).
[33] P. McFadden, R. Merrill, M. McElhinny, and S. Lee, J. Geophys. Res. **96**, 3923 (1991).
[34] G. A. Glatzmaier and P. H. Roberts, Phys. Earth Planet. Inter. **91**, 63 (1995).
[35] M. Morzfeld, A. Fournier, and G. Hulot, Phys. Earth Planet. Inter. **262**, 8 (2017).
[36] C. Grebogi, E. Ott, F. Romeiras, and J. A. Yorke, Phys. Rev. A **36**, 5365 (1987).
[37] R. Karnatak, H. Kantz, and S. Bialonski, Phys. Rev. E **96**, 042211 (2017).
[38] D. Faranda, M. Bourgoin, S. Miralles, P. Odier, J.-F. Pinton, N. Plihon, F. Daviaud, and B. Dubrulle, New J. Phys. **16**, 083001 (2014).
[39] D. Ruelle, *Chaotic Evolution and Strange Attractors*, Vol. 1 (Cambridge University Press, Cambridge, UK, 1989).
[40] V. Lucarini, D. Faranda, A. C. G. M. M. de Freitas, J. M. M. de Freitas, M. Holland, T. Kuna, M. Nicol, M. Todd, and S. Vaienti, *Extremes and Recurrence in Dynamical Systems* (Wiley, Hoboken, NJ, 2016).
[41] In fact, a preliminary analysis of this system by adding Wiener noise suggests that its invariant measure is extremely unstable to very small noise amplitude, an indicator that this system probably does not satisfy axiom A.
[42] L.-S. Young, J. Stat. Phys. **108**, 733 (2002).
[43] A. Gritsun and V. Lucarini, Physica D **349**, 62 (2017).
[44] A. Gritsun, Philos. Trans. R. Soc. A **371**, 20120336 (2013).
[45] P. Olson, R. Deguen, L. A. Hinnov, and S. Zhong, Phys. Earth Planet. Inter. **214**, 87 (2013).
[46] G. Sarson, C. Jones, and A. Longbottom, Phys. Earth Planet. Inter. **101**, 13 (1997).
[47] R. Hide, Nature (London) **222**, 1055 (1969).
[48] M. Berhanu, R. Monchaux, S. Fauve, N. Mordant, F. Pétrélis, A. Chiffaudel, F. Daviaud, B. Dubrulle, L. Marié, F. Ravelet *et al.*, Europhys. Lett. **77**, 59001 (2007).